Trends in Physical Chemistry
Vol. 16, 2016

Original Communication

Theoretical characterization of the mechanism of Alder-ene reactions

Sebastián A. Cuesta, Pamela C. Carrillo, María F. Pilaquinga and Lorena M. Meneses*
Department of Chemistry, Pontifical Catholic University of Ecuador, Quito, Ecuador.

ABSTRACT

The mechanism of Alder-ene reactions between n-hexene and heptanal and n-tetradecene and heptanal was characterized using reaction force, reaction force constant and reaction electronic flux concepts. Density-functional theory studies were performed at the B3LYP/6-311G(d,p) level. Structural analysis shows the changes in bond angles and distances throughout the reaction path. Thermodynamic analyses suggest these reactions are exothermic with activation energies between 21.1 and 34.2 kcal/mol. The proposed mechanisms follow three basic reaction steps in the transformation from reagents to products. First, the hydrogen shift from the ene to the enophile. Then, there is an electronic rearrangement produced by π and σ electrons. Finally, σ-bond formation and structural relaxation occur, leading to the final product. The mechanism found, based on the quantum descriptors, was confirmed to be the right one.

KEYWORDS: Alder-ene, reaction force, electronic flux, DFT, thermodynamics, mechanism

INTRODUCTION

In 1928, German chemists Otto Diels and Kurt Alder developed one of the most useful synthetic reactions: the Diels-Alder reaction. This reaction is used in the production of many compounds like morphine, cholesterol and cortisone [1]. One of its variations, the Alder-ene reaction, is a chemical reaction between the allylic hydrogen of an alkene (the 'ene') and a compound containing a multiple bond (the 'enophile'), in order to form a new σ-bond with the migration of the ene double bond, as shown in figure 1.

This is a group transfer pericyclic reaction, characterized by a four-electron system that goes thorough a cyclic transition state. At the transition state, the double bond is relocated and new σ-bonds are formed to get the final product. The reaction presents high activation energy due to the electronic-steric requirements to break the C-H σ-bond. Therefore, the reaction usually needs high temperatures, highly activated substrates or a Lewis acid as a catalyst.

Many theoretical and computational studies have been made on the structure of the transition state [2-5]. However, the reaction mechanism characterization has been limited to the reagents' frontier orbital interaction concepts [6].

Thus, little has been done in order to characterize Alder-ene reaction using other types of theoretical quantum descriptors, such as energy profiles, reaction force, reaction force constant and reaction electronic flux, which can provide a detailed characterization of reaction mechanisms by giving complete information of electronic changes throughout the reaction [7].

Energy profiles are dimensional diagrams that describe the evolution of the potential energy along the reaction. Also, they give information about the thermodynamics of the reaction such as the reaction enthalpy, and insights about the kinetics of the reaction through the activation energy. The Intrinsic Reaction Coordinate (IRC = ξ) shows the path that a chemical reaction follows by relating the potential energy (*E*) of reagents and products by a transition state [7].

*Corresponding author: lmmeneses@puce.edu.ec

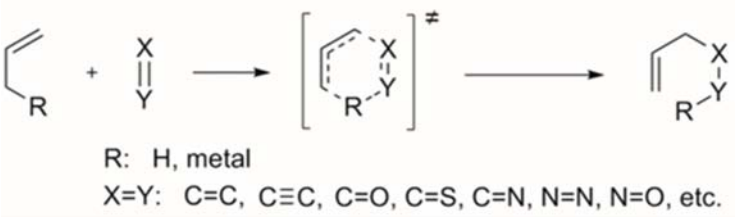

Figure 1. General representation of Alder-ene reaction between an alkene and a compound containing a multiple bond.

By taking the derivative of $E(\xi)$, the reaction force is obtained, $F(\xi) = - dE/d\xi$. This provides important information about the mechanism of a chemical process. Three regions can be distinguished between two $F(\xi)$ critical points separated by an energy barrier: a minimum (ξ_1) and a maximum (ξ_2). Those points define the reaction regions: reagents region ($\xi_R \leq \xi \leq \xi_1$), transition state region ($\xi_1 \leq \xi \leq \xi_2$) and the products region ($\xi_2 \leq \xi \leq \xi_P$), where ξ_R and ξ_P are the energies of reagents and products, respectively. In the reagents region, structural changes take place, while in the transition state region, electronic changes occur. Finally, in the products region, structural relaxation occurs, leading to products formation [8-15].

Another quantum descriptor is the reaction force constant $\kappa(\xi)$, defined as the negative derivative of the reaction force $F(\xi)$ with respect to the IRC, $\kappa(\xi) = - \partial F(\xi)/\partial \xi$ [14]. The reaction force constant profile is positive in the reagents and products regions ($\xi_R \rightarrow \xi_1$ and $\xi_2 \rightarrow \xi_P$) and negative in the transition state region ($\xi_1 \rightarrow \xi_{TS} \rightarrow \xi_2$). Maximum and minimum of $F(\xi)$ correspond to the inflexion points of the reaction force where ξ_1 and ξ_2 are zero [14].

The chemical potential is a measurement of the tendency of electrons leaving a system [16]. It can be defined by Milliken's equation for electronegativity but with the opposite sign, where A is the electronic affinity and I the system ionization potential: $\mu = -\frac{(A+I)}{2} = -\chi_M$. Applying Koopmans' approximation, $-\mu = \chi_M = \frac{(A+I)}{2} = -\frac{\varepsilon_{HOMO} + \varepsilon_{LUMO}}{2}$ is obtained, where ε_{HOMO} and ε_{LUMO} are the energies of the frontier molecular orbitals HOMO (Highest Occupied Molecular Orbital) and LUMO (Lowest Unoccupied Molecular Orbital). By evaluating μ along the reaction coordinate, the μ(ξ) profile is determined, measuring the electronic flux among molecules with different μ values. The reaction electronic flux $J(\xi)$ can be defined as $J(\xi) = -Q\frac{d\mu}{d\xi}$ where Q is the transport coefficient [15, 17, 18]. For the sake of simplicity and for allowing a proper comparison between the different reaction steps taking place in the current reaction, $Q = 1$ will be used throughout this paper to focus the analysis on the derivative of the chemical potential only [8, 17, 19, 20]. Two regions can be thermodynamically differentiated: $J(\xi) < 0$ related to spontaneous electronic density changes and $J(\xi) > 0$ associated with no spontaneous electronic density changes [15].

Therefore, the aim of this work was to perform a kinetic characterization of two Alder-ene reactions, by using reaction force, reaction force constant and reaction electronic flux concepts in the density functional theory (DFT) framework, to get a better understanding of the complete reaction mechanism.

COMPUTATIONAL METHODS

Full geometry optimizations of the ene and the enophiles were performed at the B3LYP/ 6-311G(d,p) level of theory, implemented in the GAUSSIAN 03 package of programs [21]. This method has been successfully tested by giving information about systems at the ground state and the transition state [22, 23]. Frontier orbital energies of the optimized geometries were obtained using the Hartree-Fock (HF) method and the 6-31G(d) basis set, as suggested by Vargas *et al.* [24], in order to obtain highly precise quantum descriptors. The transition states were obtained at the optimized structures with a frequency calculation, where the appearance of one imaginary frequency confirms the presence of a transition state. The values of the electronic chemical potential were obtained from the approximated expressions $\mu \approx \frac{(\varepsilon_H + \varepsilon_L)}{2}$ in terms

of the one-electron energies of the HOMO and LUMO frontier molecular orbitals, ε_H and ε_L, respectively. An IRC calculation was performed to visualize all the changes at every point of the reaction coordinate. Finally, single-point calculations of each structure along the IRC were performed at the HF/6-31G(d) level of theory, and the reaction force, reaction force constant and reaction electronic flux values were calculated.

RESULTS AND DISCUSSION

The Alder-ene reactions between n-hexene and heptanal and n-tetradecene and heptanal were studied. The reactions are shown in figure 2.

Figure 3 shows the transition states of the studied reactions. The atoms that actively participate in the reaction are labeled. In both transition states, the allylic hydrogen attached to C3 will form a σ-bond with the oxygen of the carbonyl group. The rearrangement from C1-C2 to C2-C3 will form a cyclic transition state. Also, a σ-bond is produced between C1 and C*, resulting in a group transfer product where two σ-bonds are created, resulting in one π-bond.

The reaction energy E(ξ) and the reaction force profiles F(ξ) are represented in figure 4. The energy rises until it reaches a maximum at the transition state (activation energy) and then decreases until the products-energy is reached. This can be seen at the top of figure 4. On the other hand, reaction force decreases to a minimum at ξ_1, and then it increases to a maximum at ξ_2 being zero at the transition state, to finally decrease in the product region. Observe this at the bottom of figure 4.

The reactions were exothermic, with reaction energies of ΔE^o = -12.9 kcal/mol for the reaction between n-hexene and heptanal, and ΔE^o = -12.6 kcal/mol for the reaction between n-tetradecene and heptanal. The activation energies were of E_a = 23.1 and E_a = 23.5 kcal/mol, respectively. Comparing these results with previous studies, good agreement was found. The reaction energy between ethylene and propylene calculated with a MP2 (Moller-Plesset correlation energy correction truncated at second-order) method and a 6-31G(d) basis set was ΔE^o = 29.4 kcal/mol [2]. The activation energy of E_a = 35.0 kcal/mol in the reaction between propylene and ethylene, along with E_a = 30.0 kcal/mol in the reaction between propylene and methanol, was established to be within the range of the ones found in this study [2]. The differences between them can be explained by the difference in the structures and carbon chain length. Also, it should be taken into account that the MP2 method gives less accurate results than DFT methods.

Moreover, when comparing the Alder-ene reactions studied with a Diels-Alder reaction between 1,3-butadiene and ethylene (activation energy of E_a = 25.4 kcal/mol) [25], it is confirmed that Alder-ene activation energies are slightly lower than Diels-Alder ones. In Diels-Alder reaction 6 π-electrons take part, while in the Alder-ene reactions 4 π and 2 σ-electrons take part, requiring less energy to reach the transition state [26].

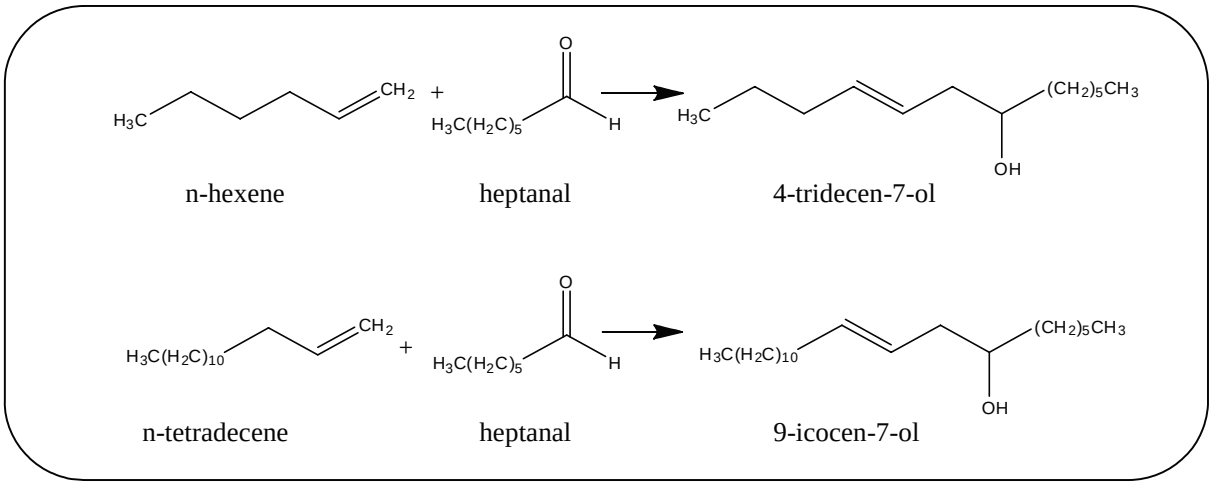

Figure 2. Alder-ene reactions studied.

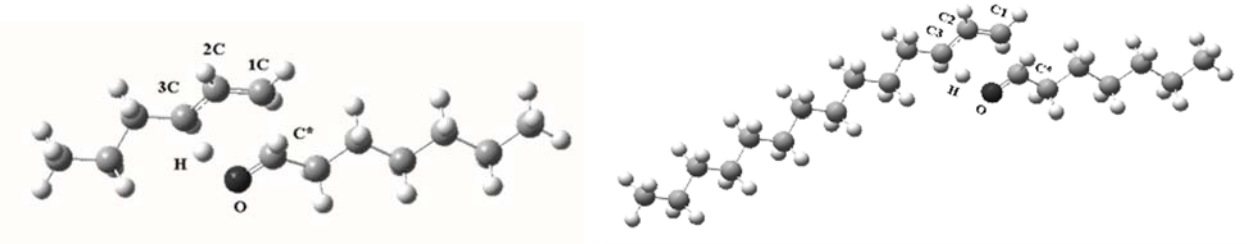

a b

Figure 3. Ball-and-stick model of the transition states in the reactions between: a) n-hexene and heptanal and b) n-tetradecene and heptanal. The gray spheres represent carbon atoms, white spheres hydrogen and black spheres oxygen.

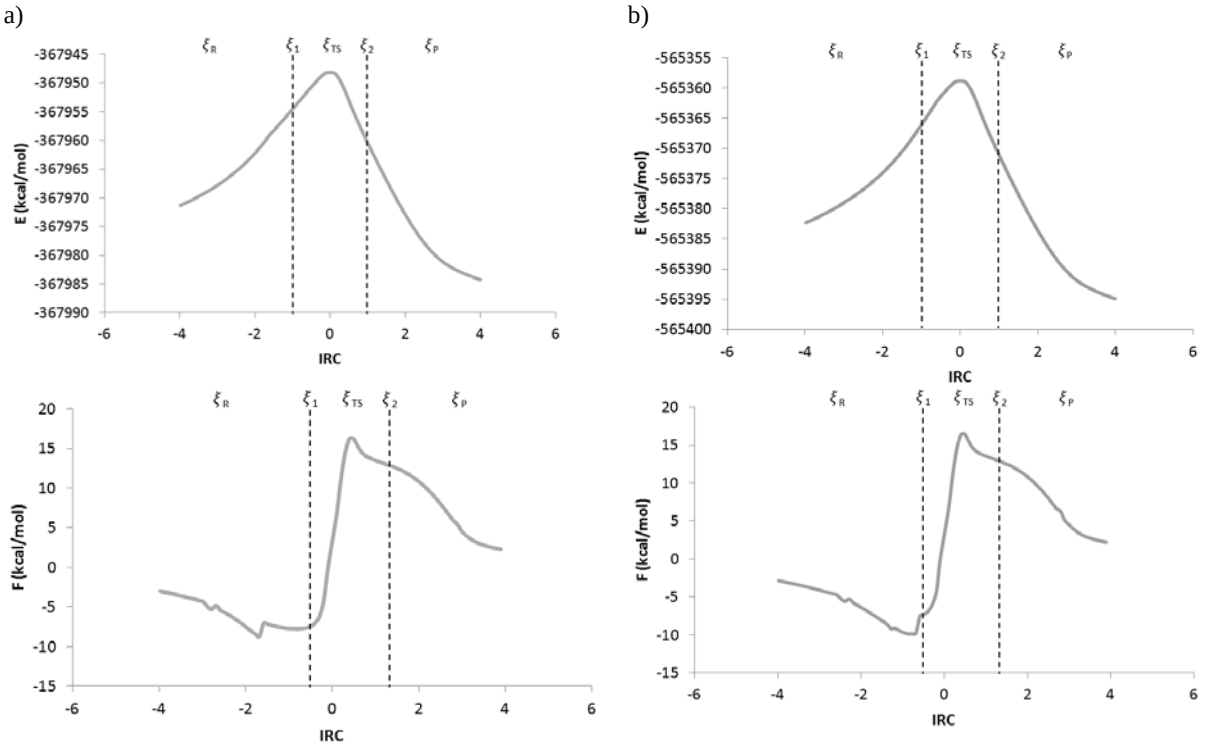

Figure 4. Energy E(ξ) and reaction force F(ξ) profiles of Alder-ene reactions. a) n-hexene-heptanal and b) n-tetradecene-heptanal.

In the reaction force profiles, $F(\xi)$, there are three important regions separated by a minimum (ξ_1) and a maximum (ξ_2). In the reagents region ($\xi_R \leq \xi \leq \xi_1$) hydrogen transfer events mainly take place between C3 and the oxygen. While in the transition state region ($\xi_1 \leq \xi \leq \xi_2$), electronic rearrangements occur. In the reactions studied, resonant bonds are formed between C2 and C3 due to the relocation of electrons. Here, interaction between HOMO orbital of the alkene and LUMO orbital of the enophile occurs. Finally, there is the products region ($\xi_2 \leq \xi \leq \xi_P$), where the electron donor and electron acceptor atoms relax and the σ-bond between the alkene and the enophile carbons are produced, forming the product. This demonstrates that Alder-ene reactions have just one elemental step [8-11].

Figure 5 shows the reaction force constant profile, $\kappa(\xi)$ and reaction electronic flux, $J(\xi)$ for the two reactions studied. The top of the figure shows that $\kappa(\xi)$ is approximately zero at the reagents and products

regions, and it reaches a minimum at the transition state structure. The bottom of the figure shows that $J(\xi)$ is around zero at the reagents and products regions. It decreases to a minimum in the transition state region.

Analyzing the reaction force constant, $\kappa(\xi)$, of the reactions studied, the negative region coincides with the one between the reaction force maximum and minimum ($\xi_1 \leq \xi \leq \xi_2$) (in figure 4). This shows that the reaction not only has a single transition state point, but has a transition state region where the system goes from activated reagents to activated products and the force constant goes from a minimum to a maximum [27]. Furthermore, the transition state region has an energy gradient of zero for all the degrees of freedom with a negative reaction force constant [14].

Figure 5 also shows the reaction electronic flux, $J(\xi)$, along the IRC of the studied reactions. In both reactions, in the reagents area ($\xi_R \leq \xi \leq \xi_1$) and in the products area ($\xi_2 \leq \xi \leq \xi_P$), there is an equilibrium region characterized by an electronic flux tending to zero. In these regions, the electronic flux is balanced, and only structural changes occur. On the other hand, the transition state region is characterized by a dramatic decrease of the electronic flux from the reagents until it reaches a minimum at the transition state structure. Then, it rises until it reaches the products region. The diagrams are similar for the two studied reactions, demonstrating that major electronic changes occur in the transition state region ($\xi_1 \leq \xi \leq \xi_2$). The perturbations found in the diagrams could be due to the energy values in the IRC path, showing a slight deviation affecting the reaction electronic flux calculation.

In the second part of the study, structural analysis of the two reactions was performed so that the changes in bond length and angles during the pericyclic process could be described (atom labeling can be seen in figure 3). Carbon atoms C1 and C2 are the ones that take part in the formation of the alkene double bond. As the reaction takes place,

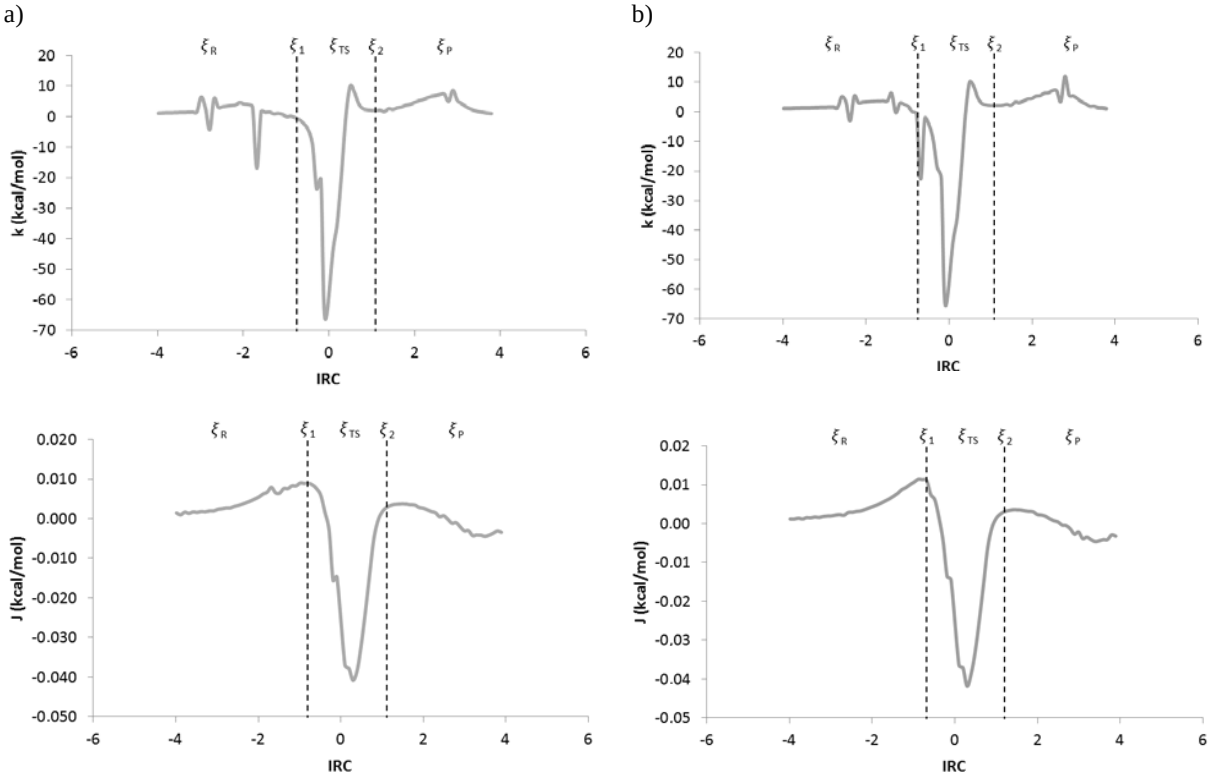

Figure 5. Reaction force constant profile, *κ(ξ)* and reaction electronic flux, *J(ξ)* of Alder-ene reactions. a) n-hexene-heptanal and b) n-tetradecene-heptanal.

the π bond of the double bond becomes a σ single bond. The distance between two atoms forming a double bond is shorter (1.34 Å) than the distance of the same atoms forming a single bond (1.50 Å) [1]. That is why the transformation from a double to a single bond is clearly observed by the increase in the bond length in the products. Changes in the distance between C2 and C3 are exactly the opposite. During the reaction, C2 and C3 change from a single bond to a double bond. Therefore, the bond length decreases during the reaction from 1.50 Å to 1.34 Å [1]. In the bond length variation between C3 and hydrogen H, the hydrogen will be released from C3 to form a hydroxyl bond with the oxygen of the enophile. As the hydrogen moves towards the oxygen, the distance between carbon and hydrogen will increase during the reaction from 1.10 Å to 2.13 Å at the end of the reaction. On the other hand, the hydrogen approaches the oxygen atom O, until they join to form the alcohol. In this case, the distance decreases from 1.93 Å to the OH bond value of 0.96 Å [1]. The distance between the aldehyde oxygen and the carbon C* shows a similar tendency as C2-C3 distances, since the changes from double to single bond occur. The distance increases as the reaction takes place from 1.21 Å to 1.42 Å at the end of the reaction. All the figures present a greater slope in the center where the IRC is close to zero. This is caused by structural and electronic changes taking place at the transition state region. A constant approach between C* and C1 is due to the formation of single bond between them. At the beginning of the reaction, the distance between carbons is 2.73 Å and at the end is a single bond length of 1.57 Å.

Angle analysis shows the angle between the carbon C1 and C2 of the alkene and the carbon C* of the enophile. The angle increases during the reaction from 88° to 108°. At the very end of the reaction a C-C bond will be formed with a tetrahedral carbon angle value of 109.4°, typical of the sp^3

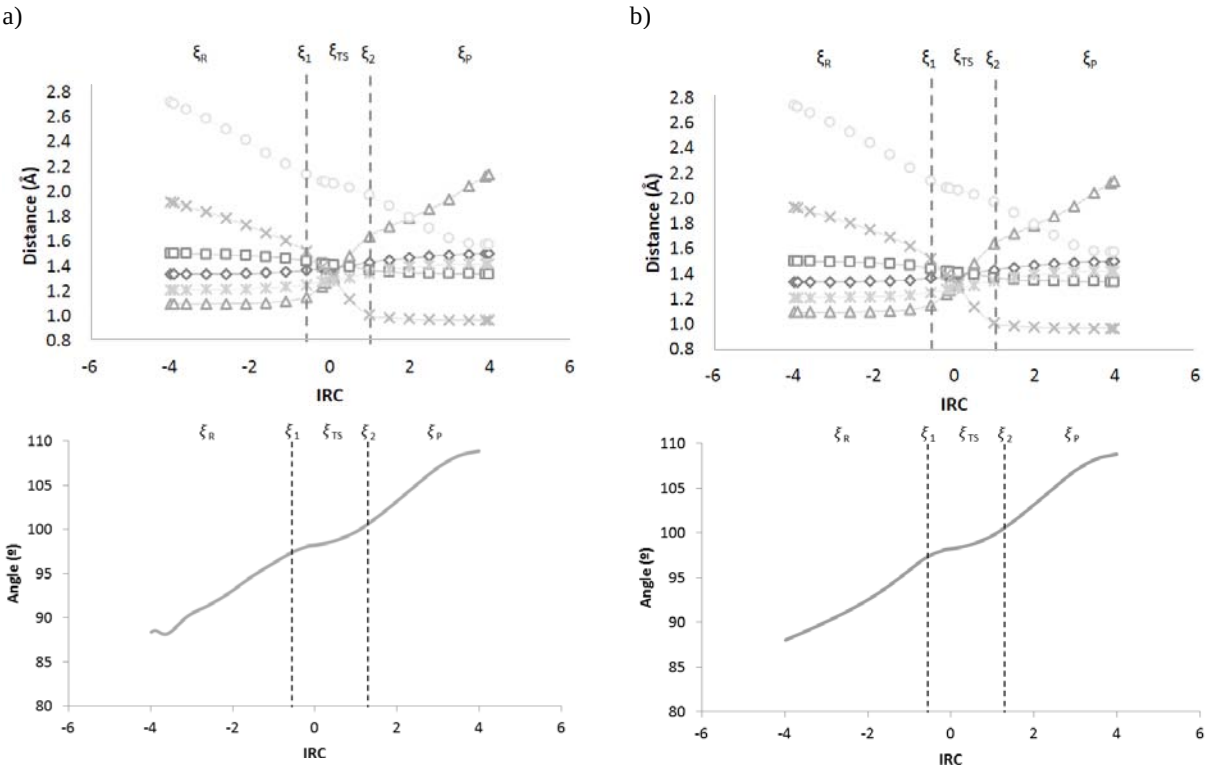

Figure 6. Structural analysis of Alder-ene reactions. a) n-hexene-heptanal and b) n-tetradecene-heptanal. C1=C2 bond length is indicated with diamonds (◊); C2-C3 with squares (□); C3-H with triangles (Δ); O-H with crosses (×); O=C* with stars (*) and C1-C with circles (○). C2-C1-C* angles were plotted in the graphs at the bottom.

hybridization [1]. All these structural changes can be observed in figure 6.

CONCLUSION

Alder-ene reactions are exothermic and have lower activation energies than most of Diels-Alder and similar reactions. The reaction mechanism along the intrinsic reaction coordinate is described, recognizing three different regions: reagents region ($\xi_R \leq \xi \leq \xi_1$), transition state region ($\xi_1 \leq \xi \leq \xi_2$), and products region ($\xi_2 \leq \xi \leq \xi_P$). By analyzing the reaction force profile, the reaction force constant, and the reaction electronic flux, we observe that the allylic hydrogen movement occurs in the reagents region; in the transition state region the electronic arrangement happens; while in the products region structural relaxation and σ-bond formation take place. Structural analysis along the reaction coordinate shows the changes in bond lengths and bond angles, providing a clear sight of the structural changes during the reaction, from the reagents to the final product. By changing the reagents, different Alder-ene reactions are studied to recognize the influence of the different structures in the reaction mechanism. It is confirmed that the mechanism found, based on the quantum descriptors, is the right one.

ACKNOWLEDGMENTS

This work was supported by DGA-PUCE grant No. I13068.

CONFLICT OF INTEREST STATEMENT

There are no conflicts of interest of any kind with the publication of this article.

REFERENCES

1. Solomons, T. W. G. and Fryhle, C. B. 2007, Organic Chemistry, 9th Edition, John Wiley & Sons, New York.
2. Deng, Q., Thomas IV, B. E., Houk, N. K. and Dowd, P. 1997, J. Am. Chem. Soc., 119(29), 6902.
3. Loncharich, R. J. and Houk, K. M. 1987, J. Am. Chem. Soc., 109(23), 6947.
4. Stephenson, L. M., Grdina, M. J. and Orfanopoulos, M. 1980, Acc. Chem. Res., 13(11), 419.
5. Yamaguchi, K., Takahara, Y., Fueno, T. and Houk, K. N. 1978, Theor. Chem. Acc.: Theory, Computation, and Modeling, 73(5-6), 337.
6. Inagaki, S., Fujimoto, H. and Fukui, K. 1976, J. Am. Chem. Soc., 98(16), 4693.
7. Fukui, K. 1981, Acc. Chem. Res., 14(12), 363.
8. Toro-Labbé, A. 1999, J. Phys. Chem. A, 103(22), 4398.
9. Jaque, P. and Toro-Labbé, A. 2000, J. Phys. Chem. A, 104(5), 995.
10. Gutiérrez-Oliva, S., Herrera, B., Toro-Labbé, A. and Chermette, H. 2005, J. Phys. Chem. A, 109(8), 1748.
11. Toro-Labbé, A., Gutiérrez-Oliva, S., Concha, M., Murray, J. S. and Politzer, P. 2004, J. Chem. Phys., 121, 4570.
12. Martínez, J. and Toro-Labbé, A. 2004, Chem. Phys. Lett., 392(1-3), 132.
13. Politzer, P., Toro-Labbé, A., Gutiérrez-Oliva, S., Herrera, B., Jaque, P., Concha, M. and Murray, J. S. 2005, J. Chem. Sci., 117, 467.
14. Jaque, P., Toro-Labbé, A., Politzer, P. and Geerlings, P. 2008, Chem. Phys. Lett., 456, 135.
15. Flores-Morales, P., Gutiérrez-Oliva, S., Silva, E. and Toro-Labbé, A. 2010, J. Mol. Structure: THEOCHEM, 943, 121.
16. Parr, R. G. and Yang, W. 1989, Density-Functional Theory of Atoms and Molecules, Oxford Science Publications, New York.
17. Herrera, B. and Toro-Labbé, A. 2007, J. Phys. Chem., 111, 5921.
18. Vogt-Geisse, S. and Toro-Labbé, A. 2009, J. Chem. Phys., 130, 244308.
19. Echegaray, E. and Toro-Labbé, A. 2008, J. Phys. Chem. A, 112, 11801.
20. Labet, V., Morell, C., Grand, A. and Toro-Labbé, A. 2008, J. Phys. Chem., 112, 11487.
21. Frish, M. J., Trucks, G. W., Schlegel, H. B., Scuseria, G. E., Robb, M. A., Cheeseman, J. R., Scalmani, G., Barone, V., Mennucci, B., Petersson, G. A., Nakatsuji, H., Caricato, M., Li, X., Hratchian, H. P., Izmaylov, A. F., Bloino, J., Zheng, G., Sonnenberg, J. L., Hada, M., Ehara, M., Toyota, K., Fukuda, R., Hasegawa, J., Ishida, M., Nakajima, T., Honda, Y., Kitao, O., Nakai, H., Vreven, T., Montgomery, Jr. J. A., Peralta, J. E., Ogliaro, F., Bearpark, M., Heyd, J. J., Brothers, E.,

Kudin, K. N., Staroverov, V. N., Kobayashi, R., Normand, J., Raghavachari, K., Rendell, A., Burant, J. C., Iyengar, S. S., Tomasi, J., Cossi, M., Rega, N., Millam, J. M., Klene, M., Knox, J. E., Cross, J. B., Bakken, V., Adamo, C., Jaramillo, J., Gomperts, R., Stratmann, R. E., Yazyev, O., Austin, A. J., Cammi, R., Pomelli, C., Ochterski, J. W., Martin, R. L., Morokuma, K., Zakrzewski, V. G., Voth, G. A., Salvador, P., Dannenberg, J. J., Dapprich, S., Daniels, A. D., Farkas, O., Foresman, J. B., Ortiz, J. V., Cioslowski, J. and Fox, D. J. 2003, GAUSSIAN 03W, Revision D 01, Gaussian Inc., Wallingford CT.

22. Meneses, L., Araya, A., Pilaquinga, F., Espín, M., Carrillo, P. and Sánchez, F. 2010, Int. J. Quantum Chem., 110, 2360.
23. Domingo, L., Aurell, M., Pérez, P. and Contreras, R. 2002, J. Phys. Chem. A, 106, 6871.
24. Vargas, R., Garza, J. and Cedillo, A. 2005, J. Phys. Chem. A, 109, 8880.
25. Bach, R. D., McDouall, J. J. and Schlegel, H. B. 1989, J. Org. Chem., 54, 2931.
26. Singh, J. 2005, Photochemistry and Pericyclic Reactions, 2nd Edition, New Delhi [s.n].
27. Toro-Labbé, A., Gutiérrez-Oliva, S., Concha, M., Murray, J. S. and Politzer, P. 2009, J. Mol. Modeling, 15(6), 707.